Published in final edited form as:

J Steroid Biochem Mol Biol. 2022 July ; 221: 106121. doi:10.1016/j.jsbmb.2022.106121.

Characterization of the major single nucleotide polymorphic variants of aldo-keto reductase 1C3 (type 5 17β-hydroxysteroid dehydrogenase)

Andrea J. Detlefsen[a], **Phumvadee Wangtrakuldee**[b], **Trevor M. Penning**[a,b,c,*]

[a]Department of Biochemistry & Biophysics, Perelman School of Medicine University of Pennsylvania, Philadelphia, PA 19104, United States

[b]Department of Systems Pharmacology & Translational Therapeutics, Perelman School of Medicine University of Pennsylvania, Philadelphia, PA 19104, United States

[c]Center of Excellence in Environmental Toxicology, Perelman School of Medicine University of Pennsylvania, Philadelphia, PA 19104, United States

Abstract

Aldo-keto reductase (AKR) 1C3, also known as type 5 17β-hydroxysteroid dehydrogenase and prostaglandin F synthase, is a member of the AKR superfamily that reduces aldehydes and ketones to primary and secondary alcohols. It plays an essential role in the peripheral formation of androgens and is implicated in several steroid hormone dependent diseases including prostate cancer, breast cancer, and polycystic ovary syndrome (PCOS). *AKR1C3* has 14 nonsynonymous single nucleotide polymorphisms (nsSNPs) with different global frequencies and ethnic distributions. Association studies support their role in disease, but a detailed functional genomic analysis of these variants is lacking. One study examined five *AKR1C3* nsSNPs for their ability to reduce exemestane, an aromatase inhibitor used to treat breast cancer, to 17β-dihydroexemestane, and reported a 17–250-fold reduction in catalytic efficiency of H5Q, E77G, K104D, and R258C variants compared to wild type (WT). This observation provided the impetus to examine the impact of these variants on AKR1C3 function. Here, we purified AKR1C3 WT, and the top four most frequently occurring nsSNPs, H5Q, E77G, K104D, and R258C, from *E. coli* to expand upon their characterization and illuminate functional differences that could affect disease outcome and treatment. While we found negligible deviations in steady state kinetics, the K104D variant showed reduced thermal stability compared to WT. The presence of $NAD(P)^+$ restored the stability of the variant. As it is unlikely that the apoenzyme will exist within the cell without cofactor bound the K104D is not expected to manifest a phenotype.

*Correspondence to: Dept. Systems Pharmacology & Translational Therapeutics, University of Pennsylvania School of Medicine, 1315 BRBII/III, 421 Curie Blvd, Philadelphia, PA 19104-6061, United States. penning@upenn.edu (T.M. Penning).

CRediT authorship contribution statement

Andrea Detlefsen: Conceptualization, Formal analysis; Investigation, Methodology, Writing – original draft, Writing – review & editing; **Phumvadee Wangtrakuldee:** Investigation, Formal analysis. **Trevor Penning:** Conceptualization, Supervision, Writing – review & editing and Funding acquisition.

Appendix A. Supporting information

Supplementary data associated with this article can be found in the online version at doi:10.1016/j.jsbmb.2022.106121.

Keywords

Enzyme kinetics; Prostate cancer; Polycystic ovary syndrome; Androgen metabolism; Exemestane; indomethacin

1. Introduction

Aldo-keto reductase (AKR) 1C3 is a member of the AKR superfamily that reduces aldehydes and ketones to primary and secondary alcohols [1]. AKR1C3 is also known as type 5 17β-hydroxysteroid dehydrogenase and prostaglandin F synthase [2]. It is responsible for the peripheral formation of androgens in target tissues and is accordingly implicated in a range of steroid hormone dependent diseases including prostate cancer [3], breast cancer [4] and polycystic ovary syndrome (PCOS) [5]. There are 14 nonsynonymous single nucleotide polymorphisms (nsSNPs) observed in *AKR1C3* [6]. These nsSNPs occur with varying global frequencies and are found in distinct distributions among continental and ethnic populations.

The most prevalent nsSNP, H5Q, occurs in a significant portion of the global population with a minor allelic frequency (MAF) of 0.42 (Fig. 1a) [6]. However, its continental prevalence is asymmetrical, where it is found in 54% of African populations but only in 14% of East Asian populations (Fig. 1a) [6]. Interestingly, prostate cancer incidence and mortality rates in the US occur in a similarly skewed distribution, where African American men experience more frequent incidence and more severe forms of the disease compared to the national average (Fig. 1b) [7,8]. By contrast, men of East Asian heritage experience significantly lower prostate cancer incidence and mortality rates compared to the national average (Fig. 1b) [7,8]. The next three most common variants, K104D, E77G, and R258C, occur with global MAFs of 0.1518, 0.0367, and 0.0325, respectively, and like H5Q appear disproportionately in different ethnic backgrounds (Table 1) [6]. The remaining *AKR1C3* nsSNPs exist in < 1% of the global population.

These nsSNPs or missense mutations could result in biochemical differences that manifest in a loss of protein function or stability within a cell [9,10]. The above nsSNPs do not occur at any obviously impactful residues of AKR1C3 such as those in the cofactor binding site, steroid binding site, or active site, however this does not nullify their potential to impact function (Fig. 2a) [1]. Notably, R258C occurs at an evolutionarily conserved amino acid, making it likely to interfere with the structural stability of AKR1C3. Additionally, mutation prediction software (PolyPhen, SIFT) [11,12], suggest that several of these nsSNPs could have deleterious effects on AKR1C3 function [6]. This evidence has led to the notion that AKR1C3 variants, particularly H5Q, could play a role in progression, severity, or response to treatment in diseases where AKR1C3 plays an integral role [13-17].

Despite the potential impact on AKR1C3 function and subsequent implications in disease, these nsSNP variants remain largely uncharacterized. One study compared the nsSNPs by their ability to reduce exemestane, an aromatase inhibitor used to treat breast cancer, to 17β-dihydroexemestane [18]. These variants were reported to have a 17–250-fold reduction in their ability to catalyze this conversion compared to WT AKR1C3, thereby prolonging the

half-life of the drug [18]. This observation provided the incentive to further investigate their functional impact. Here, we purified AKR1C3 WT, H5Q, E77G, K104D, and R258C from *E. coli* to expand upon their initial characterization and illuminate potential functional and stability differences in *AKR1C3* nsSNPs that could affect disease outcome and treatment selection.

2. Materials

Testosterone (T), Δ4-androstenedione (androst-4-ene-3,17-dione or 4AD), progesterone (P) and 20α-hydroxyprogesterone (20α-hydroxy-pregn-4-en-3-one or 20α-OH-P) were purchased from Steraloids (Wilton, NH, USA). Nicotinamide adenine dinucleotide Grade I reduced disodium salt (NADH), nicotinamide adenine dinucleotide Grade II free acid (NAD^+), nicotinamide adenine dinucleotide phosphate reduced tetrasodium salt (NADPH), and nicotinamide adenine dinucleotide phosphate oxidized disodium salt ($NADP^+$) were obtained from Roche Diagnostics (Indianapolis, IN, USA). (*S*)-(+)– 1,2,3,4-Tetrahydro-1-naphthol (*S*-tetralol) was purchased from TCI Chemicals America (Montgomeryville, PA, USA). Exemestane was purchased from Selleckchem (Houston, TX, USA). QuikChange Site-Directed Mutagenesis kits were purchased from Agilent (Santa Clara, CA, USA). *E. coli* BL21 (DE3) competent cells were purchased from New England Biolabs (Ipswich, MA, USA). DEAE-Sepharose fast flow resin, XK 26/20 column, HiTrap Blue HP 5 mL column, and N-acetyl-L-tryptophanamide (NATA) were all purchased from MilliporeSigma (Burlington, MA, USA). All other compounds were ACS grade or better and obtained from Sigma Aldrich or Thermo Fisher Scientific.

3. Methods

3.1. Purification of AKR1C3 variants

AKR1C3 WT and H5Q were overexpressed in *E. coli* BL21(DE3) using a pET-16b-vector as previously described [19]. AKR1C3 E77G, K104D, and R258C mutations were introduced into the WT using QuikChange site-directed mutagenesis. The resulting plasmids were subjected to dideoxysequencing to confirm the presence of the desired amino acid change before transformation into competent *E. coli* BL21(DE3) cells. Recombinant proteins were purified as previously described [20,21], with minor modifications. Briefly, proteins were purified through sequential FPLC steps using DEAE-Sepharose followed by Blue-Sepharose to homogeneity as determined by SDS-PAGE. Final proteins were stored in 20 mM potassium phosphate buffer pH 7.0 containing 30% glycerol, 1 mM 2-meracptoethanol and 1 mM EDTA at − 80 °C until use.

3.2. Determination of specific activity and kinetic constants by measuring the $NAD(P)^+$ dependent oxidation of S-tetralol

The specific activity of AKR1C3 was measured via oxidation of the standard substrate *S*-tetralol. *S*-tetralol oxidation was monitored spectrophotometrically by monitoring the rate of NADH generation at 340 nm using a molar extinction coefficient (ε340) of 6270 M^{-1} cm^{-1}. Specific activity measurements were made in 1 mL systems containing 3.14 mM *S*-tetralol, 2.28 mM NAD^+, 4% acetonitrile, and 0.1 M potassium phosphate (pH 7.0).

Reactions were run for 10 min at 37 °C. Specific activity measurements were performed in triplicate using five different amounts of protein (0.5, 1, 1.5, 2, and 2.5 μg) for WT and each variant. K_m and k_{cat} determinations for the NAD^+ dependent oxidation of *S*-tetralol were performed using 1.5 μg of protein in 1 mL systems containing 0–5 mM *S*-tetralol, 10 mM NAD^+, 4% acetonitrile, 0.1 M potassium phosphate (pH 7.0) and were run for 10 min at 37 °C. K_m and k_{cat} determinations for the $NADP^+$ dependent oxidation of *S*-tetralol were performed using 1.5 μg protein in 1 mL systems containing 0–750 μM *S*-tetralol, 2.5 mM $NADP^+$, 4% acetonitrile, 0.1 M potassium phosphate (pH 7) and were run for 10 min at 37 °C. All reactions were performed in triplicate and Michaelis-Menten kinetic parameters were obtained using GraphPad Prism. Statistical significance was evaluated by one-way ANOVA through GraphPad Prism.

3.3. Determination of K_d values for $NAD(P)^+$ by fluorescence titration

K_d values for the binding of cofactors to AKR1C3 variants were determined by measuring the quenching of intrinsic tryptophan fluorescence on a Hitachi F-4500 fluorescence spectrophotometer following incremental additions of $NADP^+$ (0.1–10 μM final concentration) or NAD^+ (20–1000 μM final concentration). Measurements were made in 1 mL systems containing 0.5 μM protein in 0.1 M potassium phosphate (pH 7.0) at 25 °C. The total volume change from addition of cofactors was less than 2%. Samples were excited at 290 nm and fluorescence emission was scanned from 300 to 500 nm at 240 nm/min. Untransformed fluorescence readings from the peak wavelengths of emission (320 nm, 330 nm, 335 nm, 340 nm) were averaged and plotted as percent change in fluorescence from maximum emission with no cofactor (%ΔF) versus cofactor concentration. At high concentrations, NAD^+ absorbs near the excitation wavelength of tryptophan, causing significant fluorescence quenching that is unrelated to protein-ligand binding. This is known as the inner filter effect [22,23]. To correct for the inner filter effect NAD^+ titrations were repeated as described above in the presence of 3 μM NATA, which yields a similar fluorescence signal intensity to 0.5 μM protein. The percent decrease in fluorescence intensity between each titration point with NAD^+ represents the inner filter effect [22,23]. Protein titration data were then corrected by adding the percent decrease in intensity due to the calculated inner filter effect. K_d values for NAD^+ were obtained by fitting plots of corrected fluorescence versus NAD^+ concentration using the GraphPad Prism One Site Specific binding analysis. K_d values for $NADP^+$ were calculated using the Morrison equation as described [24], which accounts for tight binding of the cofactor that was evident in these experimental conditions where the total concentration of the enzyme was within the range of the concentration of $NADP^+$ titrated into the system. Statistical significance was evaluated by one-way ANOVA through GraphPad Prism.

3.4. Discontinuous kinetic assays monitoring steroid reduction via RP-UV/HPLC

The NADPH dependent reduction of 4AD (3.5 μg of protein per reaction) and P (2.5 μg of protein per reaction) was monitored in the linear range of the velocity vs. protein concentration curve for each variant. The reduction of exemestane was performed with 10 μg of protein in accordance with the conditions reported by Platt et al. [18]. 4AD and P reduction were measured in 1 mL systems which contained 0–30 μM 4AD or P, 180 μM NADPH, 4% acetonitrile, 0.1 M potassium phosphate (pH 6.0) and were run for 1 h at

37 °C. The reduction of exemestane was measured in reactions that contained 0–100 μM exemestane, 180 μM NADPH, 4% acetonitrile, 0.1 M potassium phosphate (pH 6.0) and were run for 1 h at 37 °C. All samples were extracted twice with 1 mL ethyl acetate and dried by vacuum centrifugation before reconstitution in 100 μL of 60% acetonitrile in water. Extracted samples were run on a Waters Zorbax ODS 5 μm 4.6 × 250 mm column using a constant flow rate of 0.75 mL/min with the solvents water (A) and acetonitrile (B) for quantification of substrate and product in the reactions via reversed-phase high performance liquid chromatography linked to UV detection (RP-UV/HPLC). The method started at 15% B and increased to 75% B over 35 min. Then, it increased to 95% B over 5 min, decreased to 5% B over 1 min, held for 14 min, increased again to 15% B over 1 min and held for 4 min. Elution of 4AD, T, P, and 20α-OH-P was monitored at 242 nm, while exemestane and 17β-dihydroexemestane peaks were detected at 248 nm. Peaks were integrated and products were quantified from calibration curves constructed using authentic standards. Waters Alliance 2695 Separations Module and Waters 996 Photodiode Array Detector were used for all RP-UV/HPLC measurements. All reactions were performed in triplicate and Michaelis-Menten kinetic parameters were obtained using GraphPad Prism. Statistical significance was evaluated by one-way ANOVA using GraphPad Prism.

3.5. Dose response curves and IC_{50} values for indomethacin inhibition of AKR1C3 oxidation/reduction reactions

Dose response curves for the inhibition of AKR1C3 oxidation by indomethacin were performed by measuring the $NADP^+$ dependent oxidation of *S*-tetralol fluorometrically in a 96-well plate format. Each well contained a 200 μL system with 0.003–100 μM indomethacin dissolved in DMSO to minimize fluorescence background from solvent, 0.74 μg AKR1C3 variant, 165 μM *S*-tetralol, 200 μM $NADP^+$, a total of 2% DMSO, and 0.1 M potassium phosphate (pH 7.0). The appearance of reduced cofactor NADPH was measured using excitation at 340 nm and emission at 460 nm at 37 °C over a period of 5 min in the presence of increasing concentrations of indomethacin. The percent of the uninhibited velocity of *S*-tetralol oxidation remaining in each condition was determined relative to a control containing only the inhibitor solvent (total 2% DMSO) and plotted against the corresponding log concentration of indomethacin. Dose response curves for the inhibition of the reduction of 4AD to T by indomethacin catalyzed by the AKR1C3 variants were performed by measuring T formation with the same discontinuous RP-UV/HPLC assay previously described in kinetic measurements. Reactions were performed in 1 mL systems containing 0.002–24 μM indomethacin dissolved in acetonitrile, 3.5 μg of AKR1C3 variant, 12 μM 4AD, 180 μM NADPH, a total of 4% acetonitrile, and 0.1 M potassium phosphate (pH 6.0). Reactions were run for 1 h at 37 °C. Peaks were integrated and T formation was quantified from calibration curves constructed using authentic standards. The percent of the velocity of T formation remaining at each concentration of indomethacin was determined relative to a control reaction containing only the inhibitor solvent (total 4% acetonitrile) and plotted against the corresponding log concentration of indomethacin. All reactions were performed in triplicate, and GraphPad Prism IC_{50} analysis with x as log (concentration) was used to determine IC_{50} for each variant for each substrate. Statistical significance was evaluated by one-way ANOVA using GraphPad Prism.

3.6. Specific activity temperature dependence

The specific activity of each variant was measured following preincubation of the enzyme at 37 °C over a time course of 4 h. Enzymes were diluted to 0.5 mg/mL in 0.1 M potassium phosphate and incubated at 37 °C. After the specified time of incubation, 1.5 μg of protein was added to a 1 mL system containing 3.14 mM *S*-tetralol, 2 mM NAD^+, 4% acetonitrile, and 0.1 M potassium phosphate (pH 7.0). Specific activity was then monitored over 10 min at 37 °C as previously described. To investigate the possible cofactor-dependence of K104D stability, this assay was repeated for K104D following preincubation of 0.5 mg/mL protein in 0.1 M potassium phosphate with either 2 mM NAD^+ or 2 mM $NADP^+$. K104D preincubated with 2 mM NAD^+ was assayed as described above. After the specified time of incubation, 1.5 μg of K104D preincubated with 2 mM $NADP^+$ was added to a 1 mL system containing 300 μM *S*-tetralol, 2 mM $NADP^+$, 4% acetonitrile, and 0.1 M potassium phosphate (pH 7.0). Specific activity was then monitored as described above. Activity of each variant at each timepoint was reported as a % activity of 0 min timepoint and plotted against time of preincubation.

4. Results

4.1. H5Q variant

We originally reported the cloning of the *AKR1C3* cDNA in 1997 from a human prostate cDNA library, prior to the availability of a reference human genome. Sequence analysis revealed the presence of Q at position 5 with the sequence CAG [19]. In a separate study, our group cloned *AKR1C3* from a cDNA library generated from HepG2 cells where H was reported at position 5 with the sequence CAT [21]. Aside from this single nucleotide difference at codon 5, the two clones had identical sequences. At the time, Q5 was thought to be a possible sequencing error. However, we now know that the H5Q variant is a major nsSNP that may be present in more than 50% of the population based on ethnicity. Consequently, the prospect of cloning this variant from a cDNA library derived from a pool of RNA transcripts was highly likely. It also raises the question as to which residue should be considered WT. In this study, we performed a detailed comparison of the WT (H at codon 5) and the H5Q variant and have yet to identify any differences between the two proteins that are likely to impact the structure or function of AKR1C3.

4.2. S-tetralol oxidation and cofactor differences

WT, H5Q, E77G, K104D, and R258C AKR1C3 variants were purified with only minor impurities by overexpression in *E. coli* (Fig. 2b). The specific activity of each purified protein was measured for the oxidation of the standard substrate *S*-tetralol in the presence of the cofactor NAD^+ (Table 2). K104D and R258C had lower specific activities compared to WT, at 2.4 ± 0.22, and 2.3 ± 0.14 vs. 3.8 ± 0.35 μmol/min/mg, respectively (Table 2). H5Q and E77G did not have remarkably different specific activities compared to WT. To further investigate possible differences, a full kinetic analysis was conducted for *S*-tetralol oxidation. K104D and R258C had lower k_{cat}/K_m values than WT, at 86.3 ± 8.1 and 116 ± 19.2 compared to 152 ± 10.8 $min^{-1}mM^{-1}$ (Table 2). Similarly, K104D and R258C had notably different velocity vs. substrate concentration curves (Fig. 2c), and lower k_{cat} values (Table S1) compared to WT. However, H5Q and E77G were not found to be largely different

from WT in any kinetic parameter. This data suggests that K104D and R258C are less catalytically efficient in the NAD^+ dependent oxidation of *S*-tetralol compared to WT.

These specific activity measurements and steady state kinetic analyses were performed with the cofactor NAD^+. AKR1C3 shows dual nucleotide specificity and can utilize $NADP^+$, which binds with an affinity that is almost 1000 times greater than NAD^+ [1,2,25]. To investigate possible effects of cofactor on the steady state kinetics of *S*-tetralol oxidation the analysis was repeated with $NADP^+$. Under these conditions, the kinetic difference of K104D/R258C variants vs. WT/H5Q/E77G variants observed with NAD^+ was reduced. Velocity vs. substrate concentration curves were more comparable (Fig. 2d), and there were no fold changes in k_{cat}/K_m, k_{cat}, or K_m values across any of the variants (Table 2, Table S1).

These data suggest that K104D and R258C exhibit a cofactor preference for $NADP^+$ over NAD^+. To further investigate possible cofactor preference, the K_d of $NAD(P)^+$ was measured by quenching the intrinsic tryptophan fluorescence of the variants. There were no differences in K_d for $NADP^+$ across any variants (Table 3). However, the K_d of NAD^+ for K104D and R258C were found to be 410 ± 52 μM and 300 ± 50 μM respectively, and were significantly greater than value obtained for WT at 170 ± 26 μM (Table 3). These data support the observation that K104D and R258C display a higher preference for binding $NADP^+$ over NAD^+ compared to WT. The $NADP^+$/NADPH cofactor pair was used in subsequent reactions to ensure that any kinetic differences observed could be attributed to steroid substrate instead of the effects of NAD^+.

4.3. 4AD and P reduction by AKR1C3 variants

AKR1C3 displays both 17- and 20-ketosteroid reductase activity [1, 2]. To assess these two main activities, we measured the ability of the variants to catalyze the conversion of 4AD to T and the conversion of P to 20α-OH-P. First, an RP-HPLC method was developed to separate 4AD and T (Fig. 3a). Then, a velocity vs. substrate concentration curve was generated for each variant using a discontinuous RP-HPLC assay (Fig. 3b). There were no significant differences between variants in their steady state kinetic parameters including k_{cat}/K_m (Table 4), k_{cat}, or K_m for this reaction (Table S2). Using a similar approach, we first separated P and 20α-OH-P by RP-HPLC (Fig. 3c), and then used a discontinuous assay to generate velocity vs. substrate concentration plots (Fig. 3d). K104D had a somewhat lower k_{cat}/K_m compared to WT at 25.9 ± 4.95 vs. 43.9 ± 4.99 $min^{-1}mM^{-1}$ (Table 4). However, there were not any fold changes in k_{cat}, and K_m in variants compared to WT (Table S2).

4.4. Exemestane reduction by AKR1C3 variants

In a previous study the variants were reported to have a 17–250-fold reduction in catalytic efficiency compared to WT AKR1C3 for the 17-ketosteroid reduction of exemestane, an aromatase inhibitor [18]. This finding contrasts with the trends we observed for the *S*-tetralol, 4AD, and P substrates. To investigate this further, WT and its variants were evaluated in their ability to reduce exemestane. Exemestane was first chromatographically separated from 17β-dihydroexemestane by RP-HPLC (Fig. 4a). These conditions were used in a discontinuous RP-HPLC assay to generate velocity vs. substrate concentration for each variant (Fig. 4b). All variants had significantly reduced k_{cat}/K_m values compared to

WT, although there were no fold changes (Table 4). Overall, these results do not suggest that there are large differences in the ability of these variants to catalyze the reduction of exemestane as previously reported [18]. Variant k_{cat} and K_m values were also only slightly different from WT (Table S3).

4.5. Inhibitor sensitivity

In the context of hormone-dependent diseases, another important area of variant difference could be sensitivity to inhibition. Subsequently, AKR1C3 variants were screened for differences in inhibitor sensitivity to indomethacin, an AKR1C3 competitive inhibitor, in both oxidation and reduction reactions. WT and all the variants had similar IC_{50} values for indomethacin, close to 0.1 μM, for the oxidation of *S*-tetralol which agrees with previous measurements (Table 5) [26]. Additionally, WT and all variants had similar IC_{50} values for indomethacin in the reduction of 4AD to T (Table 5).

4.6. Specific activity temperature dependence

Missense mutations have the potential to alter protein stability [9, 10]. To investigate this, AKR1C3 variants were preincubated at 37 °C with or without $NAD(P)^+$ over the course of four hours before assaying specific activity at 37 °C. When incubated without cofactor, all variants, aside from K104D, retained maximum activity throughout the time course (Fig. 5a). By the four-hour incubation timepoint, K104D activity depreciated to roughly 50% of the activity present at time zero (Fig. 5b). In the presence of 2 mM NAD^+, activity was somewhat rescued (roughly 75% remaining at four hours) while in the presence of 2 mM $NADP^+$ the activity was fully rescued and remained at 100% over four hours (Fig. 5b). Together, these results suggest that K104D mutation results in reduced stability and that NAD^+ somewhat restores stability whereas $NADP^+$ fully preserves stability.

5. Discussion

AKR1C3 nsSNPs have been suspected to introduce biochemical differences into protein function that would explain claims from association studies that AKR1C3 variants are linked to disease progression, severity, and response to treatment [13-17]. This notion is backed by evidence that single amino acid changes can impact a protein's stability and capacity to carry out intended functions [9,10,27]. In this study, we purified and characterized the top four most frequently occurring AKR1C3 variants to illuminate potential biochemical differences. Surprisingly, we report only modest differences in reaction kinetics, inhibitor sensitivity, or stability, except for K104D, compared to WT AKR1C3. There were no significant deviations in the k_{cat}/K_m, or k_{cat} in the 17-ketosteroid reduction of 4AD to T. There were no fold-change differences in k_{cat}/K_m for the 20-ketosteroid reduction of P to 20α-OH-P.

H5Q, the most frequently occurring nsSNP with a MAF of 0.42, is reported to be associated with increased lung cancer risk due to exposure to coal combustion emissions in a Chinese population and occurrence of hormone-treatment related symptoms in a cohort of New Zealand prostate cancer patients receiving androgen deprivation therapy [16,17]. However, we found no substantial differences in steady state kinetic parameters for non-steroidal

and steroidal based substrates, stability, or inhibitor sensitivity between WT and the H5Q variant. This is not surprising, as a mutation at this position on the N-terminal loop would not be expected to cause stability changes or interfere with catalysis. The results from our biochemical characterization of this variant do not support previous studies that associated this variant with disease. These findings agree with a recent study that reported no difference in the specific activity of the H5Q variant for *S*-tetralol oxidation or its protein stability compared to WT [28]. That study also described the association of H5Q with elevated serum T levels in Japanese men undergoing androgen deprivation therapy [28]. However, since the H5Q variant was the only variable measured there may be many reasons for this false-positive association.

In one of the only functional genomic studies conducted with AKR1C3 variants, Platt et. al reported that WT AKR1C3 exhibits a 17–250-fold greater catalytic efficiency of the aromatase inhibitor exemestane to form 17β-dihydroexemestane over the same variants studied here. Theoretically, individuals with these nsSNPs would metabolize exemestane at a slower rate than WT, which could affect the half-life of the drug. If these kinetic differences were to extend beyond exemestane to androgen metabolism, they would prevent the conversion of 4AD to T or 5α-androstanedione to DHT in target tissues. These reports differ with our results that show little difference between variant catalytic efficiency for both steroidal and nonsteroidal substrates. To explore these contrasting findings, we conducted a full kinetic analysis for exemestane conversion to 17β-dihydroexemestane. We report only modest differences in the catalytic efficiency of these four AKR1C3 variants in this reaction. None of the values obtained in our study suggest that the variants are as deficient in their metabolism of exemestane as was previously reported [18]. Given the slight differences in the K_m and k_{cat} values in the reduction of exemestane by the variants, it is unlikely they will affect the clearance of the drug.

We did note some differences in the steady state kinetics of *S*-tetralol oxidation that stemmed from substituting NAD^+ for $NADP^+$. K104D and R258C had lower catalytic efficiencies with NAD^+ than WT, H5Q and E77G. However, when reactions were repeated with the preferred cofactor, $NADP^+$, these stark differences were mostly eliminated. This observation was further supported by quenching the intrinsic tryptophan fluorescence with cofactor which showed that all the variants had similar K_d values for $NAD(P)^+$, except K104D and R258C which had an increased K_d for NAD^+. These data support a difference in NAD^+ binding in K104D and R258C variants. It is noteworthy that neither of these residues reside in the cofactor binding site.

In our assessment of the temperature dependence of specific activity, K104D is less stable than WT and all other variants following preincubation at 37 °C. While the addition of NAD^+ to the K104D preincubation mixture somewhat rescued activity over the time course, only preincubation with $NADP^+$ was able to completely preserve K104D activity. This finding suggests that K104D is a destabilizing mutation and that the presence of a $NADP^+$ stabilizes the enzyme. While K104D is the second most frequently occurring nsSNP and destabilization or premature degradation could affect AKR1C3′s cellular roles, $NADP^+$/NADPH are the more physiologically relevant cofactors for the enzyme making it unlikely that this difference in stability would be impactful on androgen metabolism.

In summary, we report no major deviations in the kinetic parameters of the top four most frequently occurring AKR1C3 variants from WT. Furthermore, it is uncertain whether the small variations that were observed would result in a measurable effect on the role of AKR1C3 in disease. We did find that K104D is likely a loss of stability mutation, however the cofactor dependence of this observation makes it unlikely to impact patient outcome. Our findings are in contrast with previous claims that AKR1C3 variants, mainly H5Q, give rise to significant advantage or disadvantage over WT, and suggests that patients with AKR1C3 dependent diseases would likely be unaffected by variant status [16, 17, 28].

Supplementary Material

Refer to Web version on PubMed Central for supplementary material.

Acknowledgements

This work was supported in part by a Chemical-Biology Interface Predoctoral fellowship to AJD (T32GM133398) from the National Institute of General Medical Sciences, National Institutes of Health (NIH), Bethesda, MD United States and by NIH grants P30-ES013508 and R01-ES-029294 from the National Institute of Environmental Health Sciences, Research Triangle Park, United States awarded to TMP. The work was also supported by Philanthropic support from the Buzz Bike Challenge made to the Abramson Cancer Center, University of Pennsylvania

Abbreviations:

AKR1C3
Aldo-keto reductase 1C3

MAF
minor allelic frequency

NATA
N-acetyl-L-tryptophanamide

NADH
nicotinamide adenine dinucleotide grade I reduced disodium salt

NAD^+
nicotinamide adenine dinucleotide grade II free acid

NADPH
nicotinamide adenine dinucleotide phosphate reduced tetrasodium salt

$NADP^+$
nicotinamide adenine dinucelotide phosphate oxidized disodium salt

nsSNPs
nonsynonymous single nucleotide polymorphisms

PCOS
polycystic ovary syndrome

P
progesterone

RP-UV/HPLC
reversed-phase high performance liquid chromatography linked to UV detection

***S*-tetralol**
1,2,3,4-tetrahydro-1-naphthol

T
testosterone

WT
wild type

androst-4-ene-3,17-dione or 4AD
Δ4-androstenedione

20α-hydroxy-pregn-4-en-3-one or 20α-OH-P
20α-hydroxyprogesterone

References

[1]. Penning TM, The Aldo-Keto Reductases (AKRs): overview, Chem. Biol. Interact 234 (2015) 236–246. [PubMed: 25304492]

[2]. Penning TM, AKR1C3 (type 5 17beta-hydroxysteroid dehydrogenase/prostaglandin F synthase): roles in malignancy and endocrine disorders, Mol. Cell Endocrinol 489 (2019) 82–91. [PubMed: 30012349]

[3]. Adeniji AO, Chen M, Penning TM, AKR1C3 as a target in castrate resistant prostate cancer, J. Steroid Biochem. Mol. Biol 137 (2013) 136–149. [PubMed: 23748150]

[4]. Byrns MC, Duan L, Lee SH, Blair IA, Penning TM, Aldo-keto reductase 1C3 expression in MCF-7 cells reveals roles in steroid hormone and prostaglandin metabolism that may explain its over-expression in breast cancer, J. Steroid. Biochem. Mol. Biol 118 (3) (2010) 177–187. [PubMed: 20036328]

[5]. O'Reilly MW, Kempegowda P, Walsh M, Taylor AE, Manolopoulos KN, Allwood JW, Semple RK, Hebenstreit D, Dunn WB, Tomlinson JW, Arlt W, AKR1C3-mediated adipose androgen generation drives lipotoxicity in women with polycystic ovary syndrome, J. Clin. Endocrinol. Metabo 102 (9) (2017) 3327–3339.

[6]. Clarke L, Zheng-Bradley X, Smith R, Kulesha E, Xiao C, Toneva I, Vaughan B, Preuss D, Leinonen R, Shumway M, Sherry S, Flicek P, The 1000 Genomes Project: Data management and community access, Nat. Methods (2012) 1–4. [PubMed: 22312634]

[7]. Siegel RL, Miller KD, Jemal A, Cancer Statistics CA: A Cancer Journal for Clinicians, Wiley (2020) 7–30.

[8]. Rawla P, Epidemiology of prostate cancer, World J. Oncol 10 (2) (2019) 63–89. [PubMed: 31068988]

[9]. Chang KH, Li R, Kuri B, Lotan Y, Roehrborn CG, Liu J, Vessella R, Nelson PS, Kapur P, Guo X, Mirzaei H, Auchus RJ, Sharifi N, A gain-of-function mutation in DHT synthesis in castration-resistant prostate cancer, in Cell, NIH Public Access 154 (5) (2013) 1074–1084. [PubMed: 23993097]

[10]. Stefl S, Nishi H, Petukh M, Panchenko AR, Alexov E, Molecularmechanisms of disease-causing missense mutations, J. Mol. Biol (2013) 3919–3936. [PubMed: 23871686]

[11]. Adzhubei IA, Schmidt S, Peshkin L, Ramensky VE, Gerasimova A, Bork P, Kondrashov AS, Sunyaev SR, A method and server for predicting damaging missense mutations, Nat. Methods 7 (4) (2010) 248–249. [PubMed: 20354512]

[12]. Vaser R, Adusumalli S, Leng SN, Sikic M, Ng PC, SIFT missense predictions for genomes, Nat. Protoc 11 (1) (2016) 1–9. [PubMed: 26633127]

[13]. Figueroa JD, Malats N, García-Closas M, Real FX, Silverman D, Kogevinas M, Chanock S, Welch R, Dosemeci M, Lan Q, Tardón A, Serra C, Carrato A, García-Closas R, Castaño-Vinyals G, Rothman N, Bladder cancer risk and genetic variation in AKR1C3 and other metabolizing genes, Carcinogenesis 29 (10) (2008) 1955–1962. [PubMed: 18632753]

[14]. Cunningham JM, Hebbring SJ, McDonnell SK, Cicek MS, Christensen GB, Wang L, Jacobsen SJ, Cerhan JR, Blute ML, Schaid DJ, Thibodeau SN, Evaluation of genetic variations in the androgen and estrogen metabolic pathways as risk factors for sporadic and familial prostate cancer, Cancer Epidemiol. Biomark. Prev 16 (5) (2007) 969–978.

[15]. Liu CY, Hsu YH, Pan PC, Wu MT, Ho CK, Su L, Xu X, Li Y, Christiani DC, Kaohsiung G, Leukemia research, maternal and offspring genetic variants of AKR1C3 and the risk of childhood leukemia, Carcinogenesis 29 (5) (2008) 984–990. [PubMed: 18339682]

[16]. Lan Q, Mumford JL, Shen M, Demarini DM, Bonner MR, He X, Yeager M, Welch R, Chanock S, Tian L, Chapman RS, Zheng T, Keohavong P, Caporaso N, Rothman N, Oxidative damage-related genes AKR1C3 and OGG1 modulate risks for lung cancer due to exposure to PAH-rich coal combustion emissions, Carcinogenesis 25 (11) (2004) 2177–2181. [PubMed: 15284179]

[17]. Karunasinghe N, Zhu Y, Han DY, Lange K, Zhu S, Wang A, Ellett S, Masters J, Goudie M, Keogh J, Benjamin B, Holmes M, Ferguson LR, Quality of life effects of androgen deprivation therapy in a prostate cancer cohort in New Zealand: can we minimize effects using a stratification based on the aldo-keto reductase family 1, member C3 rs12529 gene polymorphism? BMC Urol. 16 (1) (2016) 48. [PubMed: 27485119]

[18]. Platt A, Xia Z, Liu Y, Chen G, Lazarus P, Impact of nonsynonymous single nucleotide polymorphisms on in-vitro metabolism of exemestane by hepatic cytosolic reductases, Pharmacogenet. Genomics 26 (8) (2016) 370–380.

[19]. Lin HK, Jez JM, Schlegel BP, Peehl DM, Pachter JA, Penning TM, Expression and characterization of recombinant type 2 3 alpha-hydroxysteroid dehydrogenase (HSD) from human prostate: demonstration of bifunctional 3 alpha/17 beta-HSD activity and cellular distribution, Mol. Endocrinol 11 (13) (1997) 1971–1984. [PubMed: 9415401]

[20]. Jez JM, Schlegel BP, Penning TM, Characterization of the substrate binding site in rat liver 3alpha-hydroxysteroid/dihydrodiol dehydrogenase. The roles of tryptophans in ligand binding and protein fluorescence, J. Biol. Chem 271 (47) (1996) 30190–30198. [PubMed: 8939970]

[21]. Burczynski ME, Harvey RG, Penning TM, Expression and characterization of four recombinant human dihydrodiol dehydrogenase isoforms: oxidation of trans-7, 8-dihydroxy-7,8-dihydrobenzo, Biochemistry 38 (32) (1999) 10626. [PubMed: 10441160]

[22]. Fonin AV, Sulatskaya AI, Kuznetsova IM, Turoverov KK, Fluorescence of dyes in solutions with high absorbance. Inner filter effect correction, PLoS One 9 (7) (2014), e103878. [PubMed: 25072376]

[23]. Yammine A, Gao J, Kwan AH, Tryptophan fluorescence quenching assays for measuring protein-ligand binding affinities: principles and a practical guide, Bio. Protoc 9 (11) (2019), e3253.

[24]. Jin Y, Penning TM, Multiple steps determine the overall rate of the reduction of 5alpha-dihydrotestosterone catalyzed by human type 3 3alpha-hydroxysteroid dehydrogenase: implications for the elimination of androgens, Biochemistry 45 (43) (2006) 13054–13063. [PubMed: 17059222]

[25]. Penning TM, Wangtrakuldee P, Auchus RJ, Structural and Functional Biology of Aldo-Keto Reductase Steroid-Transforming Enzymes, Endocr. Rev 40 (2) (2018) 447–475.

[26]. Liedtke AJ, Adeniji AO, Chen M, Byrns MC, Jin Y, Christianson DW, Marnett LJ, Penning TM, Development of potent and selective indomethacin analogues for the inhibition of AKR1C3 (Type 5 17beta-hydroxysteroid dehydrogenase/prostaglandin F synthase) in castrate-resistant prostate cancer, J. Med. Chem 56 (6) (2013) 2429–2446. [PubMed: 23432095]

[27]. Garte S, Gaspari L, Alexandrie AK, Ambrosone C, Autrup H, Autrup JL, Baranova H, Bathum L, Benhamou S, Boffetta P, Bouchardy C, Breskvar K, Brockmoller J, Cascorbi I, Clapper ML, Coutelle C, Daly A, Dell'Omo M, Dolzan V, Dresler CM, Fryer A, Haugen A, Hein DW, Hildesheim A, Hirvonen A, Hsieh LL, Ingelman-Sundberg M, Kalina I, Kang D, Kihara M, Kiyohara C, Kremers P, Lazarus P, Le Marchand L, Lechner MC, van Lieshout EM, London S, Manni JJ, Maugard CM, Morita S, Nazar-Stewart V, Noda K, Oda Y, Parl FF, Pastorelli R, Persson I, Peters WH, Rannug A, Rebbeck T, Risch A, Roelandt L, Romkes M, Ryberg D, Salagovic J, Schoket B, Seidegard J, Shields PG, Sim E, Sinnet D, Strange RC, Stucker I, Sugimura H, To-Figueras J, Vineis P, Yu MC, Taioli E, Metabolic gene polymorphism frequencies in control populations, Cancer Epidemiol. Biomark. Prev 10 (12) (2001) 1239–1248.

[28]. Shiota M, Endo S, Fujimoto N, Tsukahara S, Ushijima M, Kashiwagi E, Takeuchi A, Inokuchi J, Uchiumi T, Eto M, Polymorphisms in androgen metabolism genes with serum testosterone levels and prognosis in androgen-deprivation therapy, Urol. Oncol 38 (11) (2020) 849 e11–849 e18.

a.

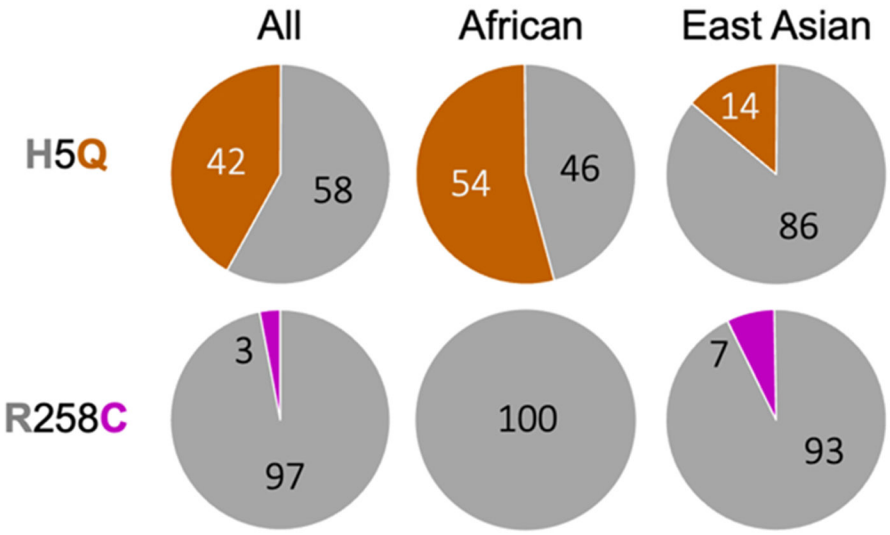

b.

	All	African American	Asian/Pacific Islander
Incidence	104.1	158.3	52.9
Mortality	19.1	38.7	8.6

Fig. 1.

(a) 1000 Genome Project minor allelic frequencies (MAFs) of AKR1C3 H5Q and R258C variants across continental populations. (b) Prostate Cancer incidence and mortality per 100,000.

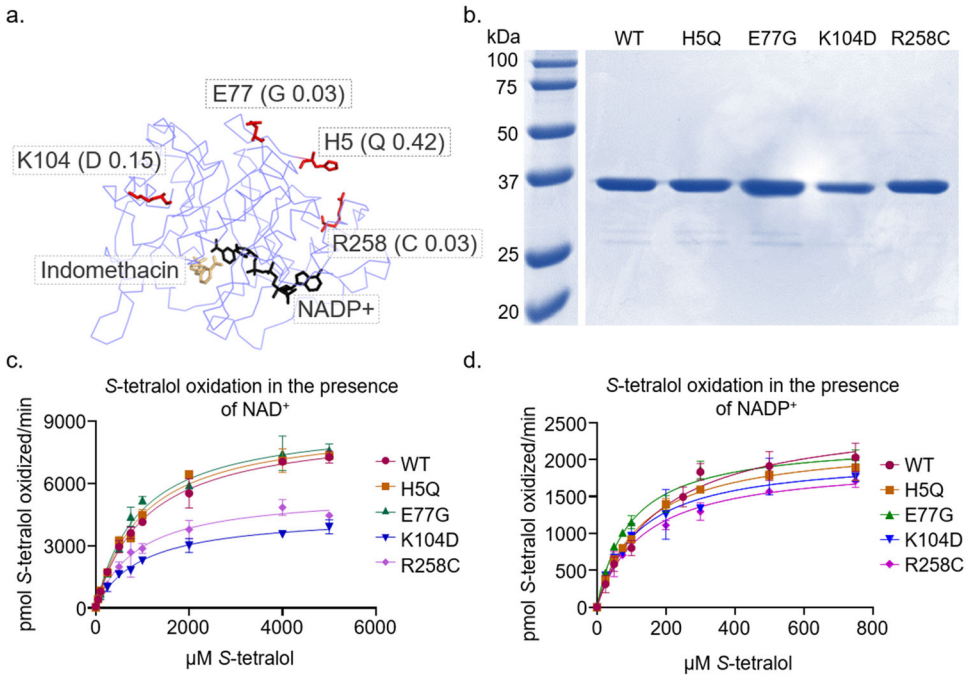

Fig. 2.

(a) Crystal structure of AKR1C3 with $NADP^+$ (black) and indomethacin (gold) (PDB: 3UG8). The locations of nsSNPs are indicated by red sticks (minor allelic frequencies of mutants are listed next to each residue); (b) Purity of AKR1C3 variants by SDS-PAGE; (c) Velocity versus substrate concentration curves for the NAD^+ dependent oxidation of *S*-tetralol catalyzed by the variants; and (d) Velocity versus substrate concentration curves for the $NADP^+$ dependent oxidation of *S*-tetralol catalyzed by the variants.

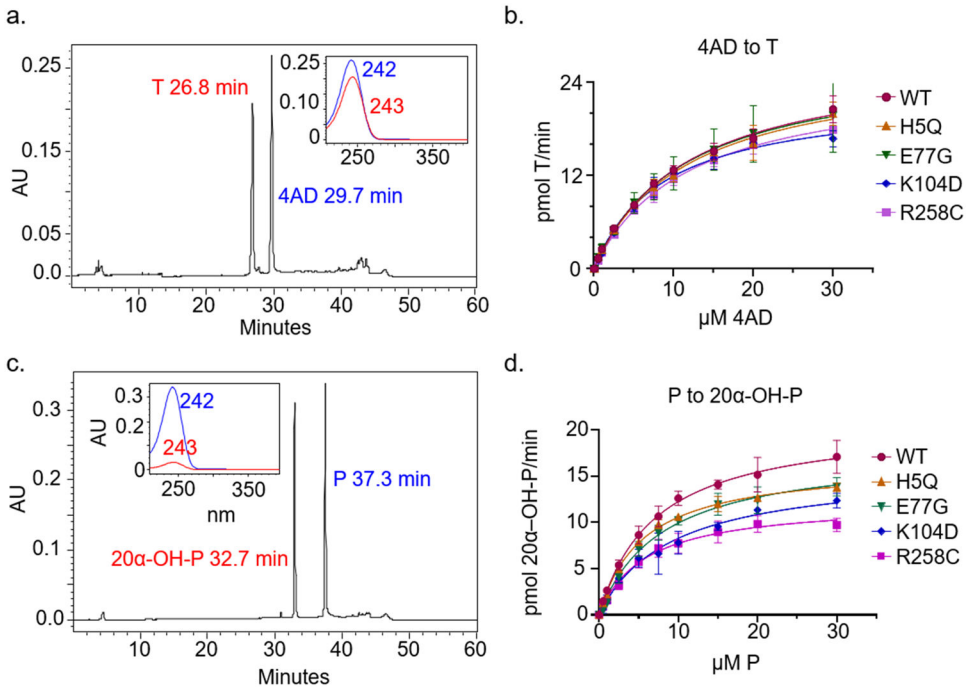

Fig. 3.

(a) RP-HPLC chromatogram showing the separation of 4 AD and T (insert shows the UV spectra for 4 AD(blue) and T (red); (b) Velocity of the conversion of 4 AD to T vs. substrate concentration catalyzed by the variants; (c) RP-HPLC chromatogram showing the separation of P and 20α-OH-P (insert shows the UV spectra for P (blue) and 20α-OH-P (red); and (d) Velocity of the conversion of P to 20α-OH-P conversion vs. substrate concentration catalyzed by the variants.

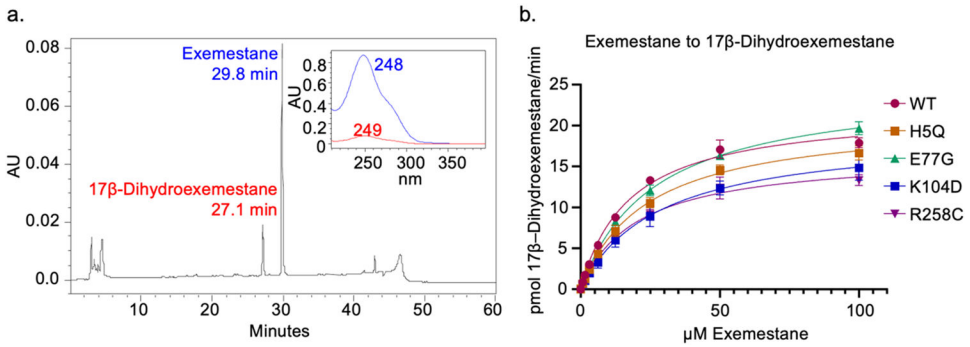

Fig. 4.

(a) RP-HPLC chromatogram showing the separation of exemestane and 17β-dihydroexemestane separation (insert panel shows the UV spectra for exemestane (blue) and 17β-dihydroexemestane (red). (b) Velocity of the conversion of exemestane to 17β-dihydroexemestane vs. substrate concentration catalyzed by the variants.

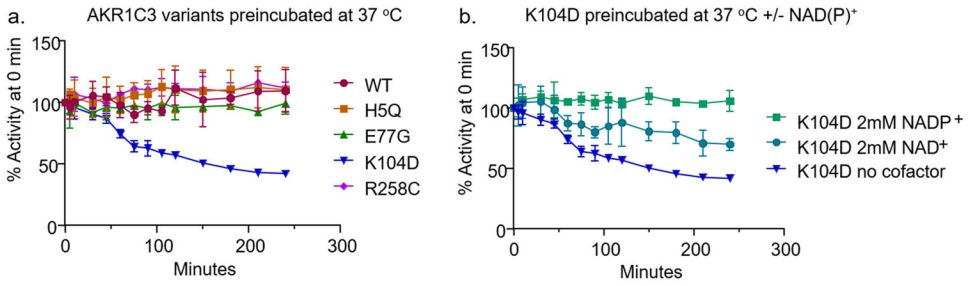

Fig. 5.

AKR1C3 variant time-dependent thermal stability at 37 °C measured as percent activity of *S*-tetralol oxidation at 0 min incubation time for (a) all variants preincubated at 37 °C alone, and (b) K104D preincubated at 37 °C alone or with 2 mM $NAD(P)^+$.

Table 1

The 1000 Genome Project MAFs of AKR1C3 variants.

Variant	NCBI identifier	Global	African	American	East Asian	European	South Asian
H5Q	rs12529	0.42	0.54	0.46	0.14	0.60	0.34
E77G	rs1155177	0.04	0.03	0.07	0	0.08	0.02
K104D	rs12387	0.15	0.13	0.19	0.14	0.15	0.18
R258C	rs62621365	0.03	0	0.12	0.70	0	0

Table 2

Variant-specific activity for the NAD^+-dependent oxidation of *S*-tetralol and catalytic efficiencies of $NAD(P)^+$-dependent reactions.

Variant	*S*-tetralol specific activity (μmol/min/mg)	*S*-tetralol NAD^+ k_{cat}/K_m ($min^{-1}mM^{-1}$)	*S*-tetralol $NADP^+$ k_{cat}/K_m ($min^{-1}mM^{-1}$)
WT	3.8 ± 0.35	150 ± 11	270 ± 45
H5Q	3.7 ± 0.31	170 ± 13	320 ± 23
E77G	3.1 ± 0.24 **	180 ± 18	440 ± 40 **
K104D	2.4 ± 0.22 ****	86 ± 8.1 ***	320 ± 60
R258C	2.3 ± 0.14 ****	120 ± 19 *	270 ± 26

For all analyses

* $p < 0.05$

** $p < 0.01$

*** $p < 0.001$

**** $p < 0.0001$.

Table 3

K_d values of $NAD(P)^+$ for AKR1C3 variants as determined by titration of the intrinsic tryptophan fluorescence.

Variant	K_d NADP+ (μM)	K_d NAD+ (μM)
WT	0.11 ± 0.017	170 ± 26
H5Q	0.12 ± 0.033	nd
E77G	0.12 ± 0.035	nd
K104D	0.10 ± 0.047	410 ± 52 **
R258C	0.20 ± 0.050	300 ± 50 *

For all analyses

* $p < 0.05$

** $p < 0.01$.

Table 4

Variant catalytic efficiencies for the NADPH dependent reduction of 4-AD P, and exemestane.

Variant	4AD k_{cat}/K_m ($min^{-1}mM^{-1}$)	P k_{cat}/K_m ($min^{-1}mM^{-1}$)	Exemestane k_{cat}/K_m ($min^{-1}mM^{-1}$)
WT	25 ± 2.4	44 ± 5.0	9.2 ± 0.68
H5Q	24 ± 3.1	44 ± 2.6	6.5 ± 0.41***
E77G	25 ± 6.3	34 ± 4.3*	7.0 ± 0.33**
K104D	27 ± 2.5	26 ± 5.0**	5.0 ± 0.59****
R258C	22 ± 1.9	31 ± 4.5*	6.0 ± 0.54****

For all analyses

* $p < 0.05$

** $p < 0.01$

*** $p < 0.001$

**** $p < 0.0001$.

Table 5

IC_{50} for indomethacin for all AKR1C3 variants.

Variant	Indomethacin IC_{50} for *S*-tetralol oxidation (μM)	Indomethacin IC_{50} for 4AD reduction (μM)
WT	0.12 ± 0.011	0.41 ± 0.031
H5Q	0.11 ± 0.0067	0.42 ± 0.031
E77G	0.12 ± 0.013	0.41 ± 0.017
K104D	0.091 ± 0.0086	0.42 ± 0.034
R258C	0.089 ± 0.019 *	0.46 ± 0.019

For all analyses

* $p < 0.05$

** $p < 0.01$

*** $p < 0.001$

**** $p < 0.0001$.